Examination of STAR fixed-target data on directed flow at $\sqrt{s_{NN}} = 3$ and 4.5 GeV

Yu. B. Ivanov [1,2,*] and M. Kozhevnikova [3,†]
[1]*Bogoliubov Laboratory of Theoretical Physics, JINR Dubna, 141980 Dubna, Russia*
[2]*National Research Center "Kurchatov Institute", 123182 Moscow, Russia*
[3]*Veksler and Baldin Laboratory of High Energy Physics, JINR Dubna, 141980 Dubna, Russia*

(Received 8 March 2024; accepted 20 June 2024; published 11 July 2024)

We present results of simulations of directed flow of various hadrons in Au + Au collisions at collision energies of $\sqrt{s_{NN}} = 3$ and 4.5 GeV. Simulations are performed within the model three-fluid dynamics and the event simulator based on it (THESEUS). The results are compared with recent STAR data. The directed flows of various particles provide information on dynamics in various parts and at various stages of the colliding system depending on the particle. However, the information on the equation of state is not always directly accessible because of strong influence of the afterburner stage or insufficient equilibration of the matter. It is found that the crossover scenario gives the best overall description of the data. This crossover equation of state is soft in the hadronic phase. The transition into QGP in Au + Au collisions occurs at collision energies between 3 and 4.5 GeV, at baryon densities $n_B \gtrsim 4n_0$ and temperatures ≈150 MeV. In-medium effects in the directed flow of (anti)kaons are discussed.

DOI: 10.1103/PhysRevC.110.014907

I. INTRODUCTION

The directed flow is one of the most sensitive quantities to the dynamics of nucleus-nucleus collisions and properties of the matter produced in these collisions. It provides information about the stopping power of the nuclear matter, its equation of state (EoS), transition to quark-gluon plasma (QGP), and more. All these issues were addressed in the analysis of the STAR data [1] obtained within the Beam Energy Scan (BES) program at the BNL Relativistic Heavy-Ion Collider (RHIC). The analysis was performed within various approaches [2–14], which include both hydrodynamic and kinetic models. An important conclusion of these studies is that the transition to the QGP is most probably of the crossover or weak-first-order type and it stars at collision energies of $\sqrt{s_{NN}} < 8$ GeV in Au + Au collisions. A promising recent development is the prediction of correlation between the directed flow and the angular momentum accumulated in the participant region of colliding nuclei [8,15–19], which allows a deeper insight into collision dynamics.

The STAR-FXT (fixed-target) data on the directed flow of identified particles at energies $\sqrt{s_{NN}} = 3$ and 4.5 GeV were recently published in Refs. [20,21]. These data were also analyzed within mostly kinetic models [11,14,22–33] in relation to various problems: the hyperon production [14,26,33], the production of light (hyper)nuclei [30,31], etc. The EoS of the matter produced in the nucleus-nucleus collisions was the prime topic of the above theoretical considerations. It was discussed mostly in terms of softness and stiffness of the EoS [11,22–24,26,29]. These studies were performed within different transport models: The relativistic version of the quantum molecular dynamics implemented into the transport code JAM [11], the hadronic transport code SMASH [22,29], the ultrarelativistic quantum molecular dynamics (UrQMD) [23,24], and a multiphase transport model [26].

All the aforementioned papers [11,22–24,26,29] reported that stiff (to a different extent) EoSs are preferable for the reproduction of the directed flow (v_1) at $\sqrt{s_{NN}} = 3$ GeV, while the v_1 data at 4.5 GeV require a softer EoS. The latter was interpreted as an indication of the onset of the phase transition into QGP. This conclusion about preference of the stiff EoS at the energy of 3 GeV appears to contradict the earlier findings. The analysis of KaoS [34] and FOPI [35] data at collision energies $E_{\rm lab} \leqslant 2A$ GeV ($\sqrt{s_{NN}} \leqslant 2.7$ GeV) within the isospin quantum molecular dynamics model led to the conclusion that the soft EoS with the incompressibility $K = 210$ MeV is strongly preferable [35–38]. Although, this energy range is somewhat below of the STAR-FXT one.

The energy range of the BNL Alternating Gradient Synchrontron (AGS), $E_{\rm lab} = 2A$–$10.7A$ GeV ($\sqrt{s_{NN}} = 2.7$–4.9 GeV), practically coincide with the currently explored STAR-FXT range. The results of the analysis of the AGS data [39,40] are more controversial. Strong preference of the soft EoS was reported in Refs. [3,4,41–43]. In Refs. [3,4], the EoS additionally softens at $\sqrt{s_{NN}} > 4$ GeV because of the onset of the deconfinement transition. However, in Ref. [44] it was found that the best description of the data on the transverse flow is provided by a rather stiff EoS at $2A$ GeV (NL3) while at higher bombarding energies ($4A$–$8A$ GeV) a medium EoS ($K = 300$ MeV) leads to better agreement with the data, while the differences in the soft-EoS and stiff-EoS transverse flows become of minor significance at $4A$–$8A$ GeV. In Ref. [45], the

*Contact author: yivanov@theor.jinr.ru
†Contact author: kozhevnikova@jinr.ru

proton flow was found to be also independent of the stiffness of the EoS, however, provided the momentum dependence in the nuclear mean fields is taken into account.

As recent studies [11,22–26,29,32] of the STAR-FXT v_1 data deduced comparatively stiff EoSs at $\sqrt{s_{NN}} = 3$ GeV, some of them predicted comparatively low baryon densities (n_B) for onset of the deconfinement transition. This transition was associated with the softening of the EoS required for v_1 reproduction at the energy of 4.5 GeV. In terms of the normal nuclear density n_0, the deduced transition densities are 3–4n_0 [22], 4n_0 [24], 2.5n_0 [25], 3–5n_0 [26], $n_B >$ 2–3n_0 [29], and 5n_0 [32]. The model of three-fluid dynamics (3FD) [46,47] predicts that the deconfinement transition starts at approximately $n_B >$ 4–5n_0 at temperatures 100–150 MeV for the crossover EoS. However, the STAR-FXT data on the directed flow of identified particles at energies $\sqrt{s_{NN}} = 3$ and 4.5 GeV have not yet been fully considered within the 3FD model, with the exception of the proton and Λ-hyperon data at 3 GeV, which were analyzed with respect to the light (hyper)nuclei production [30,31].

In view of the above reviewed developments, the debate about the EoS stiffness and onset of the QGP transition is far from complete. A more extended discussion of the EoS constraints deduced from the directed-flow analysis can be found in a recent review [48].

In the present paper, we present results of calculations of the directed flow of various hadrons at energies $\sqrt{s_{NN}} = 3$ and 4.5 GeV and compare them with recent STAR-FXT data [20,21]. The calculations are performed within the 3FD model [46,47] and also within the three-fluid hydrodynamics-based event simulator extended by UrQMD final state interactions (THESEUS) [49–51]. The THESEUS simulations are intended to study the effect of the UrQMD afterburner stage on the directed flow. We present some conclusions that can be drawn from agreement or disagreement of the calculated results with the data.

II. 3FD MODEL AND THESEUS GENERATOR

The 3FD model [46,47] simulates nonequilibrium at the early stage of nuclear collisions by means of two counterstreaming baryon-rich fluids. The third (fireball) fluid accumulates newly produced particles, dominantly populating the midrapidity region. These fluids, i.e., the projectile (p), target (t), and fireball (f), are governed by conventional hydrodynamic equations coupled by friction terms in the right-hand sides of the Euler equations. The friction terms describe the energy-momentum exchange between the fluids.

The hydrodynamic evolution ends with the freeze-out procedure described in Refs. [52,53]. The freeze-out criterion is $\varepsilon < \varepsilon_{\rm frz}$, where ε is the total energy density of all three fluids in their common rest frame. The freeze-out energy density $\varepsilon_{\rm frz} = 0.4\,{\rm GeV/fm}^3$ was chosen mostly on the condition of the best reproduction of secondary particle yields for all considered EoSs, see [46]. The 3FD freeze-out includes an antibubble prescription, preventing formation of bubbles of frozen-out matter inside the dense matter while it is still hydrodynamically evolving. The matter is allowed to be frozen out only if either (a) it is located near the border with the vacuum (this piece of matter gets locally frozen out) or (b) the criterion $\varepsilon < \varepsilon_{\rm frz}$ is met in the whole system (the whole system gets instantly frozen out). The thermodynamic quantities of the frozen-out matter are recalculated from the in-matter EoS, with which the hydrodynamic calculation is performed, to the hadronic gas EoS. This is done because a part of the energy is still accumulated in collective mean fields at the freeze-out instant. This mean-field energy should be released before switching to the hadronic cascade in order to preserve energy conservation.

The output of the model is recorded in terms of Lagrangian test particles (in terms of the numerical scheme "particle-in-cell"), i.e., fluid droplets for each fluid α (= p, t, or f). Each particle contains information on space-time coordinates of the frozen-out matter, proper volume of the test particle, hydrodynamic velocity, temperature, baryonic, and strange chemical potentials. The THESEUS generator transforms the 3FD output into a set of observed particles, i.e., performs a particlization.

The 3FD model does not include any kinetic afterburner stage. The THESEUS event generator [49–51] does include the afterburner stage that is described by the UrQMD model. The afterburner stage is of prime importance for collisions at lower energies, where there is no clear rapidity separation between participant and spectator nucleons at the freeze-out. When the time for the nuclei to pass each other becomes long relative to the characteristic time scale for the participant evolution, the interaction between participants and spectators (so-called shadowing) becomes important [54–56]. In particular, the squeeze-out effect [57–59] is the consequence of this shadowing, i.e., results from blocking of the expanding central blob by the spectator matter. This shadowing only partially is taken into account within the 3FD evolution because the central fireball remains to be shadowed even after the freeze-out while particles escape from this fireball without interacting with spectators in the 3FD model.

The afterburner stage should, in principle, correct this deficiency. However, it does not do it completely. The reason is that the THESEUS artificially assigns *the same time instant* to all produced particles before proceeding to the afterburner, while different parts of the system are frozen-out at *different time instants* in 3FD. A time-extended transition from hydrodynamic evolution to afterburner dynamics would need treatment of the interaction of the kinetic afterburner phase with still hydrodynamically evolving matter. This is a difficult task both technically and conceptually. The same time that is artificially assigned to all generated particles before the UrQMD stage is the way to avoid this difficulty, however at the expense of skipping this hydrokinetic interaction. The lack of this interaction is the prime reason of shortcoming of the THESEUS afterburner.

At lower collision energies, participants are frozen out earlier than spectators. The spectators evolve slower because of the lower excitation energy and hence require longer time before the freeze-out. Therefore, the afterburner skips the stage of shadowing the afterburner expansion of the central fireball by spectators still being in the hydrodynamic phase. It means that the evolution of the frozen-out participants is effectively stopped until the spectators also become frozen out. When the

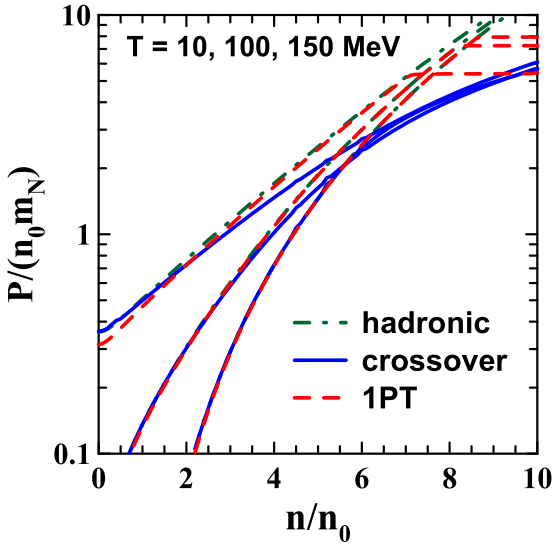

FIG. 1. Pressure (scaled by product of the normal nuclear density, $n_0 = 0.15$ 1/fm^3, and the nucleon mass, m_N) at three temperatures, $T = 10$, 100, and 150 MeV (from bottom upwards for corresponding curves), as function of the net baryon density (scaled by n_0) for the hadronic, crossover, and 1PT EoSs.

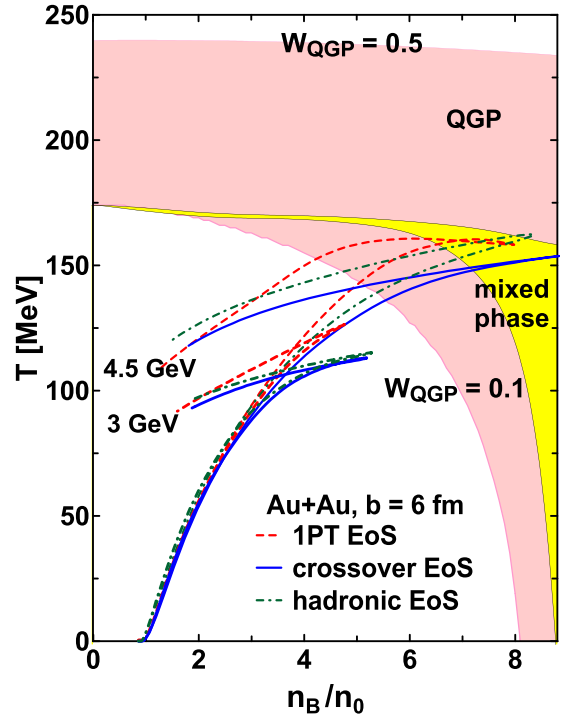

FIG. 2. Dynamical trajectories of the matter in the central cell of the colliding Au + Au nuclei in semicentral collisions (impact parameter is $b = 6$ fm) at energies $\sqrt{s_{NN}} = 3$ and 4.5 GeV. The trajectories are plotted in terms of the baryon density (n_B, scaled by the normal nuclear density n_0) and temperature T. The trajectories are presented for the three EoSs. The mixed phase of the 1PT EoS is displayed by the shadowed region marked as "mixed phase". The wide shadowed area displays the region of the crossover EoS between the QGP fractions $W_{\rm QGP} = 0.1$ and 0.5.

spectators also become frozen out, they have already partially passed the expanding central fireball. Thus, the shadowing by spectators turns out to be reduced compared to what it would be if the entire collision process were kinetically treated, like in UrQMD or JAM.

The 3FD model has been extensively used to simulations of Au + Au collisions at AGS energies, which almost coincide with the STAR-FXT ones. Quantities, which are low sensitive to the afterburner stage, were well reproduced by the 3FD simulations. These are various bulk observables [47,60,61], proton directed [3,4] and elliptic (at higher AGS energies) [59] flow, bulk properties, and directed flow of light (hyper)nuclei at $\sqrt{s_{NN}} = 3$ GeV [30,31]. Problems with reproduction of the elliptic flow of protons and light nuclei at $\sqrt{s_{NN}} = 3$ GeV in Ref. [30] are related to the aforementioned deficiency of the isochronous particlization in THESEUS. Precisely the same parameters of the 3FD model as those in Refs. [3,4,30,31,47,60,61] are used in the present simulations.

III. EQUATIONS OF STATE

The 3FD model is designed to work with different EoSs. Three different EoSs are traditionally used in the 3FD simulations: a purely hadronic EoS [62] and two EoSs with deconfinement transitions [63], i.e., an EoS with a first-order phase transition (1PT EoS) and one with a smooth crossover transition. While the hadronic EoS is quite flexible, i.e., it allows for changes of incompressibility, the EoSs with deconfinement transitions are strictly tabulated. These EoSs are illustrated in Fig. 1. As seen, all three EoSs are similar in the hadronic phase. Note that the displayed version of the hadronic EoS is characterized by incompressibility $K = 190$ MeV. The simulations below are performed with this version of the hadronic EoS. The crossover pressure starts to deviate from the hadronic one at $n_B > 4$–$5n_0$ at temperatures 100–150 MeV that are typical for the collisions at STAR-FXT energies, see Fig. 2.

Dynamical trajectories of the matter in the central cell of the colliding Au + Au nuclei in semicentral collisions ($b = 6$ fm) at energies $\sqrt{s_{NN}} = 3$ and 4.5 GeV are presented in Fig. 2 in terms of the baryon density and temperature. Evolution starts from the normal nuclear density and zero temperature and then follows an almost universal trajectory for some time. Shortly before reaching the turning point, at which density and temperature are maximal, the matter in this central cell becomes equilibrated, as it was demonstrated in Ref. [64], and therefore the temperature takes its conventional meaning. The turning points at the energy of 3 GeV only touches the QGP region according to the crossover EoS, see Fig. 1. The same time the 4.5-GeV trajectories fall well into the crossover QGP region and even enter the the 1PT mixed phase. The trajectories for different EoSs move away from each other at higher densities and temperatures. In particular, it demonstrates that the hadronic EoS and the 1PT one are not identical in the whole hadronic phase.

The crossover and 1PT phase diagrams require some comments. The QCD lattice calculations demonstrated that the transition into QGP at zero baryon chemical potential is a

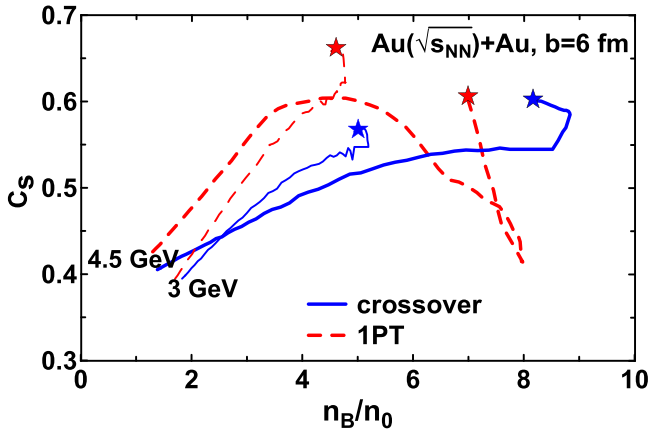

FIG. 3. Evolution of the isentropic speed of sound (c_s) as function of the baryon density (n_B, scaled by the normal nuclear density n_0) along the dynamical trajectories displayed in Fig. 2. The evolution is displayed from the instants (indicated by star symbols) when the matter is sufficiently equilibrated. The trajectories are presented for the 1PT EoS and crossover EoS. The trajectories for collisions at $\sqrt{s_{NN}} = 3$ and 4.5 GeV are displayed by thin and thick lines, respectively.

smooth crossover [65]. Due to that, the transition temperature is ambiguous because different definitions can lead to different values for it. Observables related to chiral symmetry result in the transition temperature around 155–160 MeV [66]. As seen from Fig. 2, the transition regions at zero baryon density (i.e., chemical potential) in EoSs of Ref. [63] are located at noticeably higher temperatures than 155–160 MeV. This happens because the EoSs of Ref. [63] were fitted to the old, still imperfect lattice data [67–69]. Moreover, the crossover transition constructed in Ref. [63] is very smooth. The hadronic fraction survives up to very high temperatures. In particular, this is seen from Fig. 2: the fraction of the quark-gluon plasma ($W_{\rm QGP}$) reaches a value of 0.5 only at very high temperatures. Such a smooth crossover is also used in the PHSD model (parton-hadron-string dynamics) [70]. However, this version of the crossover [63] certainly contradicts results of the lattice QCD calculations at zero chemical potential, where a fast crossover was found [65]. However, the aforementioned shortcomings are not severe for the present simulations at relatively low collision energies, because the system evolution takes place in the region of high baryon densities, where the EoS is not known from the first principles.

In order to illustrate the difference between the 1PT EoS and crossover EoS in regions probed by the semicentral collisions at $\sqrt{s_{NN}} = 3$ and 4.5 GeV, in Fig. 3 we present the evolution of the isentropic speed of sound (c_s) as a function of the baryon density along the dynamical trajectories displayed in Fig. 2:

$$c_s = \left(\frac{\partial P}{\partial \varepsilon}\right)_{\text{along trajectory}}, \tag{1}$$

where P and ε are the pressure and energy density, respectively. We do not show c_s for hadronic EoS to avoid an overcrowding of the figure. The evolution is displayed beginning from instants (indicated by star symbols) when the matter is sufficiently equilibrated, i.e., the difference between the longitudinal ($P_{\rm long}$) and transverse ($P_{\rm tr}$) pressures,

$$P_{\rm long} = T_{zz}, \ \text{(along the beam direction)}, \tag{2}$$

$$P_{\rm tr} = (T_{xx} + T_{yy})/2 \tag{3}$$

does not exceed 10% [64]. These pressures are defined in terms of the total energy-momentum tensor

$$T^{\mu\nu} \equiv T_{\rm p}^{\mu\nu} + T_{\rm t}^{\mu\nu} + T_{\rm f}^{\mu\nu} \tag{4}$$

being the sum of conventional hydrodynamical energy–momentum tensors of separate fluids

$$T_\alpha^{\mu\nu} = (\varepsilon_\alpha + P_\alpha) u_\alpha^\mu u_\alpha^\nu + g^{\mu\nu} P_\alpha, \tag{5}$$

where u_α^μ stands for the μ component of the hydrodynamic four-velocity of the α fluid. The equilibration in the central region is attained shortly before reaching the turning point [64], at which density and temperature are maximal, see Fig. 2. After that the evolution of the unified fluid is approximately (up to viscous-like dissipation) isentropic [71] and therefore Eq. (1) takes the meaning of the isentropic speed of sound.

As seen from Fig. 3, the 1PT EoS and crossover EoS at the expansion stages of the semicentral collisions are indeed different, which was indicated already in Fig. 2. It is remarkable that the softest-point region is probed at collisions at 4.5 GeV within the 1PT scenario. Indeed, the sound speed reaches minimum in the turning point of the 1PT trajectory. However, this softest-point region does not greatly affect the directed flow, as we will see below, since only the central region of the entire system falls within this softest-point region and only for a short time. The strong effect on v_1 occurs at higher collision energies, i.e., around energy of ≈8 GeV [3,4], when a large part of the matter falls within this softest-point region and for a longer time.

At the same time, the softest point affects the midrapidity region of the rapidity distribution of net protons in central collisions approximately at the same energy (4.9 GeV) [47,72,73]. It happens because a more extended region falls within this softest-point range in central collisions and because the effect is located in the midrapidity that is closely related to the central region of the system.

IV. DIRECTED FLOW

The calculated directed flow of protons, pions, Λ hyperons, and (anti)kaons as a function of rapidity in semicentral Au + Au collisions at collision energies of $\sqrt{s_{NN}} = 3$ and 4.5 GeV are presented in Figs. 4 and 5, respectively. These calculations were performed in the 3FD model without any afterburner and within THESEUS (i.e., with the UrQMD afterburner). The collision centrality was associated with the corresponding mean impact parameter by means of the Glauber simulations based on the nuclear overlap calculator [74]. Of course, this an approximate way to simulate the experimental centrality selection. Nevertheless, it captures the main trends of directed flow. The results are compared with STAR data [20,21].

As seen, the proton v_1 flow is well reproduced with and without afterburner. The afterburner slightly improves the

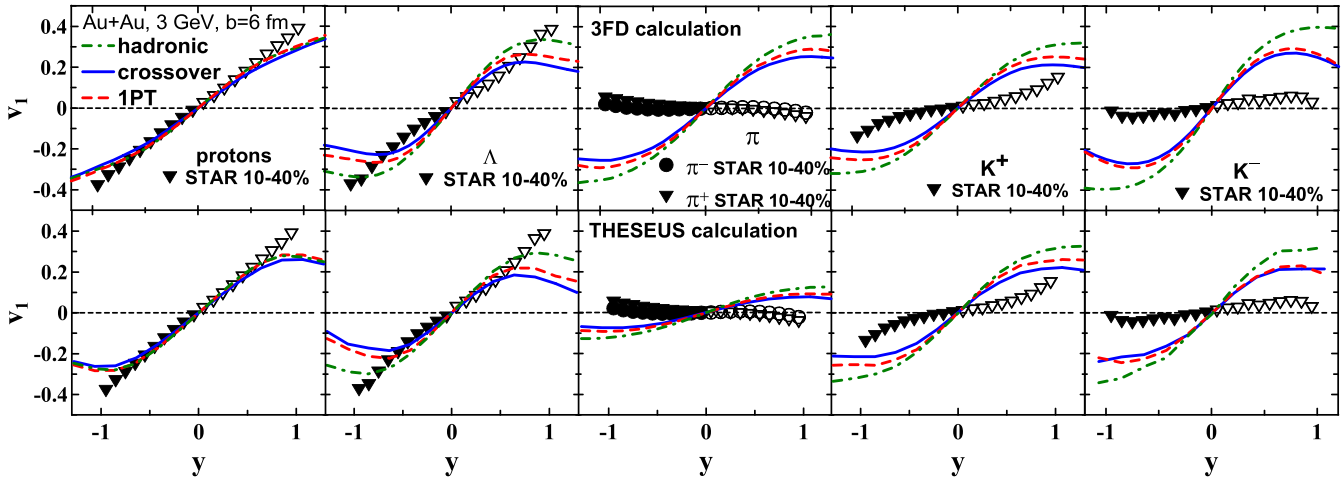

FIG. 4. Directed flow of protons, pions, Λ hyperons, and kaons as function of rapidity in semicentral ($b = 6$ fm) Au + Au collisions at collision energy of $\sqrt{s_{NN}} = 3$ GeV. Results are calculated within the 3FD model (upper raw of panels) and the THESEUS (lower raw of panels) with hadronic, 1PT, and crossover EoSs. STAR data are from Ref. [21].

description at 4.5 GeV, while worsens it at forward/backward rapidities at 3 GeV without changing the midrapidity slope. The midrapidity proton flow turns out to be almost independent of the used EoS even at 4.5 GeV, where the QGP transition already takes place, see Fig. 2. This is because the proton flow is formed at the early stage of the collision [75–77]. At considered collision energies, this stage is developed in the hadronic phase for all considered EoSs, see Fig. 2, where all considered EoSs are very similar, see Fig. 1. Moreover, the stopping power of the matter, i.e., friction forces of the 3FD model [47], are identical in the hadronic phase for all considered scenarios. Consequently, the flow appears to be quite independent of the used EoS even at 4.5 GeV. Note that the proton directed flow does depend on the EoS at the BES RHIC energies [2–4], where the transition to QGP occurs already the early stage of the collision. Figure 6 illustrates the description of the old E895 data [39] in the same collision energy range. These data are presented in terms of transverse flow defined as [78]

$$\langle P_x \rangle(y) = \frac{\int d^2p_T \; p_x \; E \; dN/d^3p}{\int d^2p_T \; E \; dN/d^3p}, \tag{6}$$

where p_x is the transverse momentum of the proton in the reaction plane, $E\,dN/d^3p$ is the invariant momentum distribution of protons with E being the proton energy, and integration runs over the transverse momentum p_T. This is done because

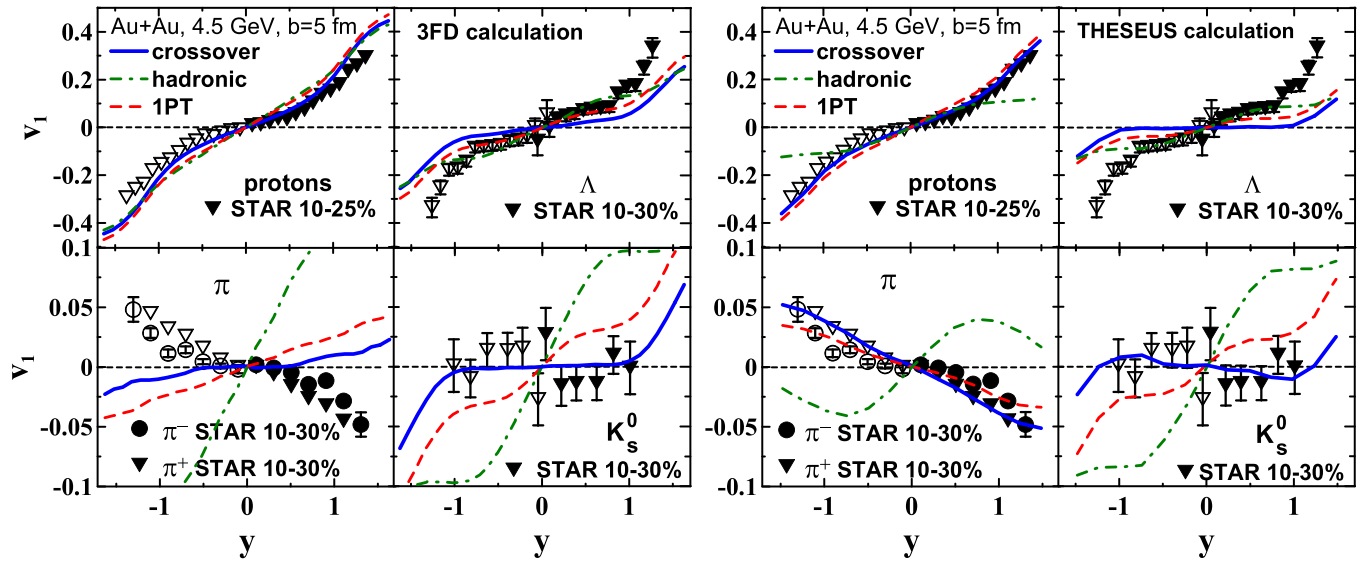

FIG. 5. Directed flow of protons, pions, Λ hyperons, and kaons (K^0 short) as function of rapidity in semicentral ($b = 5$ fm) Au + Au collisions at collision energy of $\sqrt{s_{NN}} = 4.5$ GeV. Results are calculated within the 3FD model (left block of panels) and the THESEUS (right block of panels) with hadronic, 1PT, and crossover EoSs. STAR data are from Ref. [20].

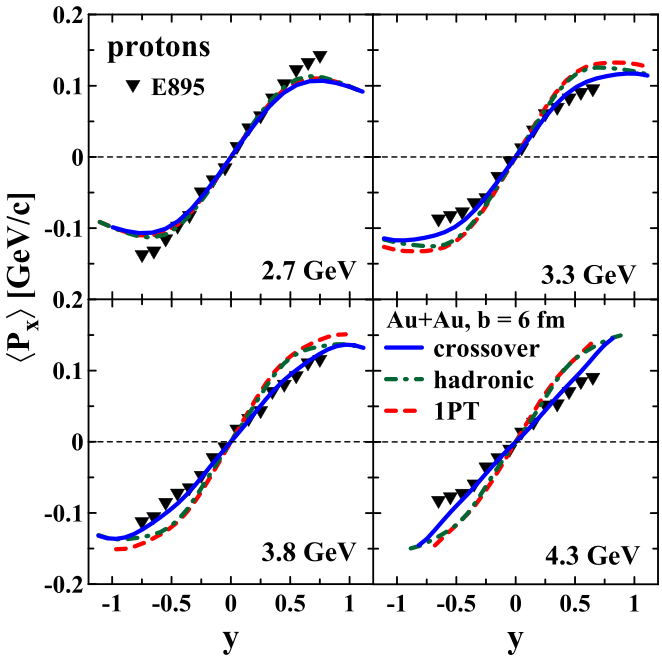

FIG. 6. Transverse flow of protons as function of rapidity in semicentral ($b = 6$ fm) Au + Au collisions at collision energies of $\sqrt{s_{NN}} = 2.7$–4.3 GeV ($E_{\rm lab} =$ $2A$, $4A$, $6A$, and $8A$ GeV). Results are calculated within the 3FD model with hadronic, 1PT, and crossover EoSs. E895 data are from Ref. [39].

the E895 data in terms of $v_1(y)$ raised many questions, as was discussed in Ref. [3] in detail. In addition, they contradict the new STAR-FXT data. As seen from Fig. 6, the crossover EoS gives almost perfect description of the proton transverse flow in the midrapidity regions. This gives hope that the future STAR-FXT proton data at the energies between 3 and 4.5 GeV will be also well reproduced with the crossover scenario. The dependence on the EoS is quite moderate, similar to that at 3 and 4.5 GeV in Figs. 4 and 5.

The Λ flow turns out to be more sensitive to the EoS, see Figs. 4 and 5, because Λs are produced in highly excited but still baryon-rich regions of the colliding system. Note that the same freeze-out energy density can be achieved by means of either high baryon density at moderate temperature or high temperature at moderate baryon density, the latter we refer as the highly excited but still baryon-rich regions. These regions are formed later, when the temperature reaches high values, see Fig. 2. The afterburner stronger affects evolution in these regions. It reduces the midrapidity slope of the Λ flow, making the crossover EoS somewhat preferable at 3 GeV, while the hadronic EoS turns out to be preferable at 4.5 GeV. In view of this sensitivity to the afterburner, definite conclusions on the EoS relevance can hardly be made based on the Λ flow.

The meson flow probes dynamics in highly excited baryon-rich and baryon-depleted regions of the system. Again, the same freeze-out energy density can be achieved by means of either high baryon density at moderate temperature, or high temperature at moderate baryon density, as is the case in the baryon-depleted regions. The highly excited baryon-depleted regions are formed even later than the excited baryon-rich regions, when the transverse expansion already dominates. Relative contributions of the baryon-rich and baryon-depleted regions to nucleon and meson production may be different. Therefore, the mesonic flow does not necessary follow the nucleon pattern. Nevertheless, the mesonic flow is very similar to the baryon one after the 3FD stage at 3 GeV, see Fig. 4, which indicates that mesons are mostly produced from decays of baryonic resonances.

At 4.5 GeV, the mesonic flow substantially differ from the baryon one, see Fig. 5. This difference at 4.5 GeV concerns only the EoSs involving the transition to the QGP, whereas the hadronic EoS results in the mesonic flow being similar to the baryon one. This implies that in the QGP-transition scenarios the relative contribution of the baryon-depleted regions becomes higher because of thermal production of mesons and mesonic resonances. The EoS becomes softer in the QGP and hence the pressure causing the directed flow is reduced. To a greater extent, this concerns the mesonic flow formed at the QGP stage of the collision. Therefore, the mesonic flow may indicate the transition to the QGP. However, there are other circumstances that may prevent us from drawing definite conclusions from the mesonic flow. One of them is the afterburner.

The pion flow is strongly affected by the afterburner. If the 3FD-calculated pion flow hardly resembles the corresponding data, after the afterburner stage, it almost perfectly describes these data at 4.5 GeV within the crossover and 1PT scenarios. The hadronic scenario evidently fails to reproduce the pion flow at 4.5 GeV. The afterburner even changes the sign of the midrapidity slope of the crossover and 1PT flows at 4.5 GeV. Note that the 3FD model and hence THESEUS do not distinguish positive, neutral, and negative pions. Therefore, the calculated pion flow refers to the flow of all pions. This strong dependence on the afterburner is a consequence of the shadowing discussed in Sec. II. At 3 GeV, the afterburner shifts the 3FD-calculated flow closer to the data but still not enough to reproduce them. This insufficient effect of the afterburner is a result of the shortcoming of the THESEUS afterburner discussed in Sec. II: The afterburner skips the stage of shadowing the afterburner expansion of the central fireball by spectators still being in the hydrodynamic phase. At 4.5 GeV, this skipped stage is already of miner importance because the time for the nuclei to pass each other becomes shorter relative to the time scale of the participant evolution.

The K^+ directed flow is not changed by the afterburner stage because of small cross sections of their interactions with other hadrons. Indeed, the kaon-nucleon cross section is about 10 mb, while the nucleon-nucleon one is about 40 mb [38,79,80]. Indeed, at somewhat lower energies ($2A$ GeV) it was concluded that after their production the K mesons suffer not more than one rescattering before escaping [81,82]. At the energy of 3 GeV ($\approx 3A$ GeV), higher densities are achieved in the collisions and therefore rescatterings become more frequent, however not frequent enough to thermalize the kaon. This explains why the calculated flow (on the assumption of the kaon thermalization) is so different from the data, see Fig. 4.

At slightly higher collision energy of 3.85 GeV ($6A$ GeV), the rescatterings of the kaons with the nucleons in the dense

matter already cause them to flow in the direction of the nucleons, as it was reported in Ref. [41]. Thus, the transition from rare-collisional to collisional regime occurs in the considered energy range. At the energy of 4.5 GeV, the kaons can be considered well thermalized at the late stage of nuclear collision, however the afterburner still does not affect the flow, as seen from Fig. 5.

At the same time, the K^- directed flow at 3 GeV is reduced by the afterburner because the NK^- cross section is of the order of 40 mb or even higher at low relative NK^- energies [38,79,80]. However, the calculated K^- flow is still essentially stronger than the experimental one. Apparently, this is a result of the aforementioned shortcoming of the THESEUS afterburner, i.e., a lack of shadowing of the central fireball by still hydrodynamically evolving spectators.

Within the 3FD model, we calculate $v_1(y)$ for K^0_s mesons in terms of those for K^0 and $\bar{K}^0$ as follows:

$$v_1^{K0s}(y) = \left(v_1^{K0}(y)\frac{dN^{K0}}{dy} + v_1^{\bar{K}0}(y)\frac{dN^{\bar{K}0}}{dy} \right) \Bigg/ \left(\frac{dN^{K0}}{dy} + \frac{dN^{\bar{K}0}}{dy} \right), \tag{7}$$

where dN^{K0}/dy and $dN^{\bar{K}0}/dy$ are rapidity distributions of the K^0 and $\bar{K}^0$ mesons. Equation (7) does not imply that K^0_s consists of K^0 and $\bar{K}^0$ in this proportion. It only means that K^0_s mesons originate from K^0 and $\bar{K}^0$ mesons that are emitted from the interaction region. These K^0 and $\bar{K}^0$ mesons keep their momenta and thus their flow pattern after escaping from the interaction region. Therefore, the corresponding fractions of produced K^0_s mesons carry these K^0 and $\bar{K}^0$ flow patterns. The $\bar{K}^0$ number is about 20% of that of K^0 at 4.5 GeV.

The directed flow of K^0_s mesons at 4.5 GeV strongly depends on the EoS and moderately depends on the afterburner. This moderate dependence on the afterburner is a consequence of the large fraction of K^0 mesons in produced K^0_s. The K^0 mesons are practically unaffected by the afterburner. Therefore, the K^0_s directed flow is a good probe of the hot and dense stage of the collision. As seen from Fig. 5, the crossover EoS is certainly preferable for reproduction of the data.

Thus, the directed flows of various particles provide information on dynamics in various parts and at various stages of the colliding system depending on the particle. However, the information on the EoS is not always directly accessible because of strong influence of the afterburner stage or insufficient thermalization of kaons. The crossover scenario gives the best overall description of the data, of course, with all reservations regarding the above-mentioned difficulties in applying the model.

V. DIRECTED FLOW OF KAONS

The kaons deserve a separate discussion. As has been mentioned above, the afterburner does not affect the flow of kaons because of small cross sections of their interactions with other hadrons but noticeably changes the antikaon flow at 3 GeV, see Fig. 4. It is instructive to consider the kaon and antikaon flows at 4.5 GeV, in spite of absence of the corresponding data.

The directed flow of kaons, antikaons and K^0_s mesons as function of rapidity in semicentral ($b = 5$ fm) Au + Au collisions at a collision energy of $\sqrt{s_{NN}} = 4.5$ GeV is presented in Fig. 7. The flows of kaons and antikaons are marked as (K^0, K^+) and $(\bar{K}^0, K^-)$, respectively, because the 3FD model does not distinguish the corresponding mesons. The kaon flow again turns out to be insensitive to the afterburner.

The flow of antikaons is enhanced by the afterburner, contrary to the reduction of the antikaon flow at 3 GeV. Notably, midrapidity slopes of the kaon and antikaon flow are of the opposite sign for the crossover and 1PT EoSs while they are both non-negative within the hadronic scenario. Apparently, the antiflow of the antikaons is again related to the aforementioned shadowing of the decay of central blob by the spectator matter. This shadowing is present already in the 3FD stage of the evolution, as seen from the upper row of panels in Fig. 7. The afterburner additionally enhances this shadowing and hence the antiflow, see the middle row of panels in Fig. 7. These opposite signs of the midrapidity slopes of the kaon and antikaon flows can be considered as a prediction for the flow at 4.5 GeV.

In-medium modifications of kaons are discussed in connection with chiral symmetry restoration and neutron star properties, see review [83]. In Refs. [38,41,80,84], it was found that in-medium modifications of kaons are very important for description of the kaon observables, in particular, the kaon directed flow. It was reported that these in-medium effects can even change the midrapidity slope of the kaon flow at the energy of 3.85 GeV (6*A* GeV) [41], i.e., in the energy range we consider here.

In the relativistic mean-field approximation for the baryon degrees of freedom [85,86], the in-medium (anti)kaon energy reads

$$E(\mathbf{p}) = \left[m_K^2 + \mathbf{p}^2 - \frac{\Sigma_{KN}}{f_K^2}\rho + \left(\frac{3}{8}\frac{n}{f_K^2}\right)^2 \right]^{1/2} \pm \frac{3}{8}\frac{n}{f_K^2}, \tag{8}$$

where $\mathbf{p}$ is the three-momentum of the (anti)kaon, the upper(lower) sign refers to $K(\bar{K})$:

$$n = \sum_B \langle \bar{B}\gamma^0 B\rangle, \quad \rho = \sum_B \langle \bar{B}B\rangle$$

are the proper baryon density and scalar baryon density, respectively, which are sums over various baryons B. Numerical values of the kaon decay constant, $f_K = 106$ MeV, and the kaon-nucleon sigma term, $\Sigma_{KN} = 350$ MeV, are taken from Ref. [38]. The term proportional to Σ_{KN} results from the attractive scalar interaction due to explicit chiral symmetry breaking.

The above expression was derived for the so-called *s*-wave interaction. Importance of *p*-wave kaon-baryon interactions was indicated in Refs. [87,88]. The treatment of the kaon-baryon interaction beyond the mean-field approximation, i.e., with the *G*-matrix approach [80,83], also turned out to be important. Therefore, Eq. (8) can only serve as a basis for the estimation of the in-medium effects in (anti)kaon production.

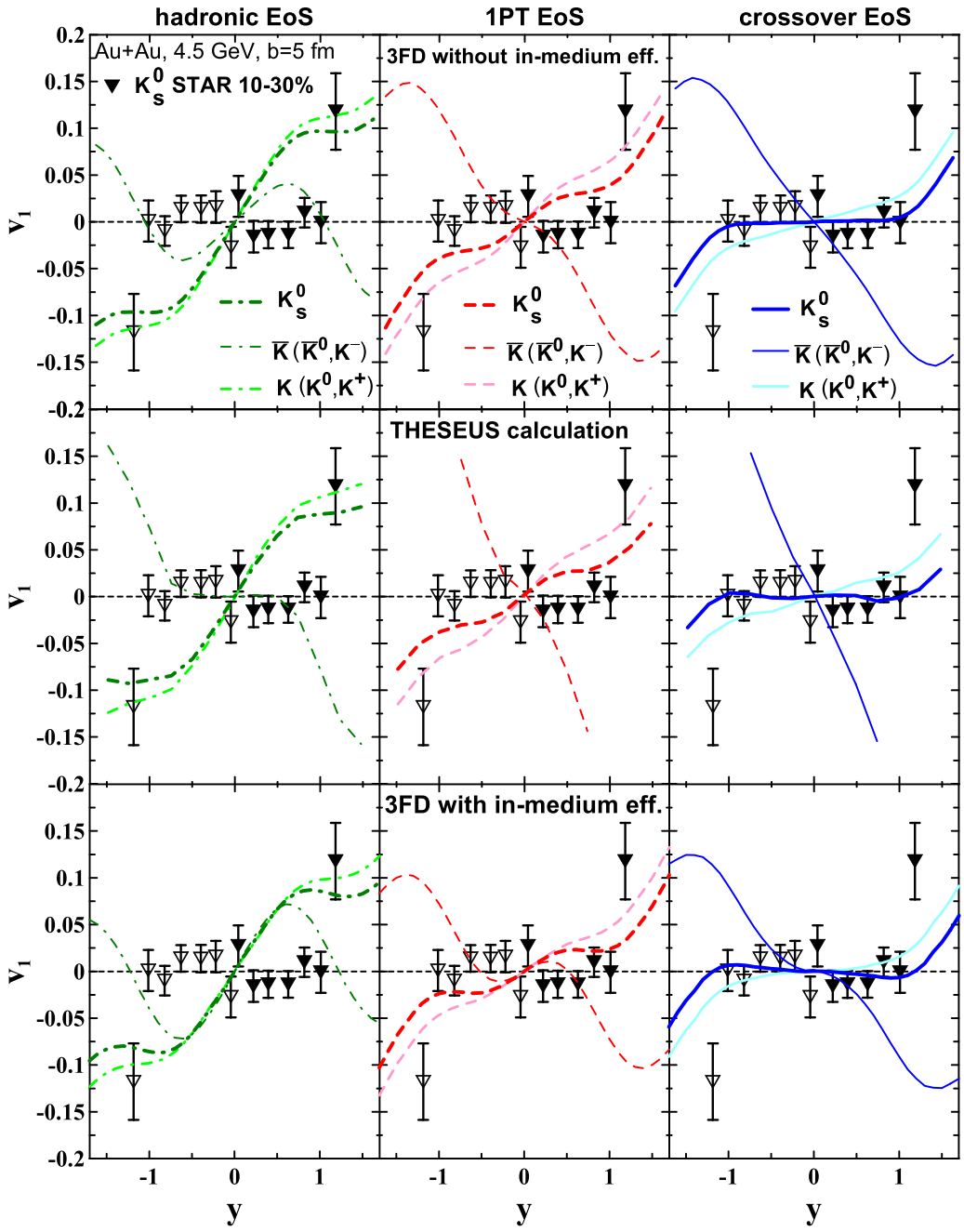

FIG. 7. Directed flow of kaons, antikaons, and K^0_s mesons as a function of rapidity in semicentral ($b = 5$ fm) Au + Au collisions at collision energy of $\sqrt{s_{NN}} = 4.5$ GeV. Results are calculated within THESEUS (the middle row of panels) and also within the 3FD model with (the lower row of panels) and without (the upper row of panels) in-medium modifications of (anti)kaons. STAR data are from Ref. [20].

Below we use Eq. (8) for this purpose. The same form of the in-medium kaon energy was used in Ref. [41].

The version of the UrQMD that is implemented in THESEUS is not suitable for treatment of the medium modified kaons. Therefore, we study the in-medium effects within the 3FD model. The masses and chemical potentials of (anti)kaons were modified at the freeze-out stage. Results of the 3FD calculation of the directed flow taking into account the in-medium kaon modification at collision energy of $\sqrt{s_{NN}} = 4.5$ GeV are shown in the lower row of panels of Fig. 7. As seen, the effect of this in-medium modification is quite moderate. However, it slightly improves the agreement with the K^0_s data within the 1PT EoS and especially the crossover scenario. This improvement is practically the same as that resulted from the afterburner. It is remarkable that the change of the antikaon flow due to the in-medium effects is opposite to that caused by the afterburner.

As seen from Fig. 8, the effect of the in-medium modifications of (anti)kaons is also small contrary to that found in Refs. [38,41,80,84]. Apparently, this is because the kaons

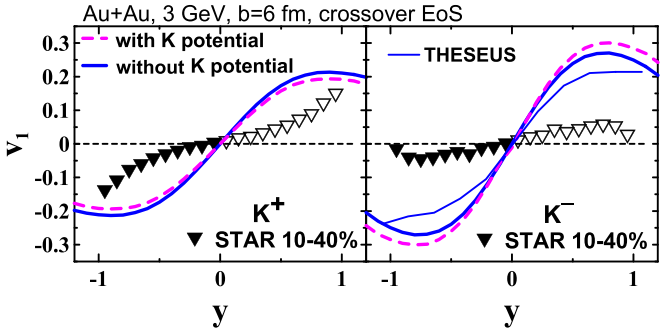

FIG. 8. Directed flow of kaons (left panel) and antikaons (right panel) as function of rapidity in semicentral ($b = 6$ fm) Au + Au collisions at collision energy of $\sqrt{s_{NN}} = 3$ GeV. Results are calculated with (with K potential) and without (without K potential) in-medium modifications of (anti)kaons for the crossover EoSs. STAR data are from Ref. [20].

were incompletely equilibrated in the matter in kinetic simulations of Refs. [38,41,80,84] and hence the in-medium effect was accumulated throughout the evolution of the system. In the 3FD simulations they are completely equilibrated and the in-medium modifications appear only at the freeze-out, leaving them insufficient time to manifest themselves. Therefore, the present calculation should be considered as a lower estimate of the in-medium effects for kaons. Again the in-medium modifications and the afterburner result in opposite changes in the antikaon directed flow. Only the afterburner decreases and the in-medium modification increases the flow, contrary to that at 4.5 GeV. This is because there is the normal flow at 3 GeV instead of antiflow at 4.5 GeV.

We can conclude that the directed flow of kaons or K_s^0 is a promising probe of the EoS at hot and dense stage of the collision at 4.5 GeV because it is not affected by the afterburner stage. At 3 GeV, the kaons do not appear to be fully equilibrated in matter and therefore do not reflect the EoS of the matter. The antikaon flow is also a good EoS probe, which is however strongly modified during the afterburner evolution.

VI. SUMMARY

The directed flow of various hadrons at energies $\sqrt{s_{NN}} =$ 3 and 4.5 GeV were calculated and compared with recent STAR-FXT data [20,21]. The calculations were performed within the 3FD model [46,47] and also within the THESEUS generator [49–51] in order to to study the effect of the UrQMD afterburner stage on the directed flow. Three different EoSs are used in the simulations: a purely hadronic EoS [62] and two EoSs with deconfinement transitions [63], i.e., an EoS with a strong first-order phase transition and one with a smooth crossover transition.

At these collision energies, the time for the nuclei to pass each other is long relative to the time scale of the participant evolution and therefore the interaction between participants and spectators (shadowing) is important. In particular, the squeeze-out effect is a consequence of this shadowing. This shadowing only partially is taken into account within the 3FD evolution because the central fireball remains to be shadowed even after the freeze-out. Therefore, the afterburner stage becomes of prime importance.

The afterburner shifts the 3FD-calculated flow closer to the data but still not enough to reproduce the pion and antikaon flow at 3 GeV. This insufficient effect of the afterburner results from shortcoming of its isochronous initialization: The afterburner skips the stage of shadowing of the post-freeze-out expansion of the central fireball by spectators still hydrodynamically evolving.

The directed flows of various particles provide information on dynamics in various parts and at various stages of the colliding system depending on the particle. However, the information on the EoS is not always directly accessible because of strong influence of the afterburner stage or insufficient equilibration, as it happens with kaons at 3 GeV. Based on these simulations, the following conclusions were drawn:

(i) The proton flow is formed at the early stage of the collision, where the matter is not yet equilibrated. Therefore, it probes the properties of this nonequilibrium matter rather than its EoS that implies the equilibrated matter. The proton flow is well reproduced within all three considered scenarios and is practically independent of the afterburner.

(ii) The Λ flow turns out to be more sensitive to the EoS because Λs are produced in highly excited but still baryon-rich regions of the colliding system. These regions are formed later, when the temperature reaches high values. The afterburner stronger affects evolution in these regions.

(iii) The meson flow probes dynamics of highly excited baryon-rich and baryon-depleted regions of the system. The highly excited baryon-depleted regions are formed even later than the excited baryon-rich regions, when the transverse expansion already dominates.

(iv) The pion flow is strongly affected by the afterburner. This strong dependence on the afterburner is a consequence of the shadowing.

(v) The directed flow of kaons or K_s^0 is a promising probe of the EoS at hot and dense stage of the collision at 4.5 GeV because it is not affected by the afterburner stage. At 3 GeV, the kaons do not appear to be fully equilibrated in matter and therefore do not reflect the EoS of the matter. The antikaon flow is also a good EoS probe, which is however strongly modified during the afterburner evolution.

In conclusion, the crossover scenario gives the best overall description of the data, of course, with all reservations regarding the above-mentioned difficulties in applying the model. This crossover EoS is soft in the hadronic phase. This result agrees with that in Refs. [3,4,41,42] but is in contrast to Refs. [11,22–24,26,29], where stiff EoSs were found being preferable for the reproduction of the directed flow at 3 GeV. The conclusion about the preference of the stiff EoS [11,22–24,26,29] was mostly based on the proton

flow, which is formed at the early nonequilibrium stage of the collision. Therefore, the proton flow is a combined result of the EoS and the stopping power of the matter. Different combinations of the EoS and the stopping power can properly describe the proton flow. Directed flows of different hadrons, as well as other bulk observables should be considered together to decouple effects of the EoS and the stopping power.

Within the preferred crossover scenario, the transition into QGP in Au + Au collisions occurs at collision energies between 3 and 4.5 GeV, at baryon densities $n_B \gtrsim 4n_0$ and temperatures ≈150 MeV. This implies that the EoS additionally softens at 4.5 GeV. This softening and hence transition into QGP at 4.5 GeV agrees well with conclusions made in Refs. [11,22–24,26,29].

ACKNOWLEDGMENTS

Fruitful discussions with D. N. Voskresensky are gratefully acknowledged. This work was carried out using computing resources of the federal collective usage center "Complex for simulation and data processing for mega-science facilities" at NRC "Kurchatov Institute" [89]. and computing resources of the supercomputer "Govorun" at JINR [90].

[1] L. Adamczyk *et al.* (STAR Collaboration), Beam-energy dependence of the directed flow of protons, antiprotons, and pions in Au+Au collisions, Phys. Rev. Lett. **112**, 162301 (2014).
[2] V. P. Konchakovski, W. Cassing, Y. B. Ivanov, and V. D. Toneev, Examination of the directed flow puzzle in heavy-ion collisions, Phys. Rev. C **90**, 014903 (2014).
[3] Y. B. Ivanov and A. A. Soldatov, Directed flow indicates a cross-over deconfinement transition in relativistic nuclear collisions, Phys. Rev. C **91**, 024915 (2015).
[4] Y. B. Ivanov and A. A. Soldatov, What can we learn from the directed flow in heavy-ion collisions at BES RHIC energies? Eur. Phys. J. A **52**, 10 (2016).
[5] J. Steinheimer, J. Auvinen, H. Petersen, M. Bleicher, and H. Stöcker, Examination of directed flow as a signal for a phase transition in relativistic nuclear collisions, Phys. Rev. C **89**, 054913 (2014).
[6] Y. Nara, H. Niemi, A. Ohnishi, and H. Stöcker, Examination of directed flow as a signature of the softest point of the equation of state in QCD matter, Phys. Rev. C **94**, 034906 (2016).
[7] C. Shen and S. Alzhrani, Collision-geometry-based 3D initial condition for relativistic heavy-ion collisions, Phys. Rev. C **102**, 014909 (2020).
[8] S. Ryu, V. Jupic, and C. Shen, Probing early-time longitudinal dynamics with the Λ hyperon's spin polarization in relativistic heavy-ion collisions, Phys. Rev. C **104**, 054908 (2021).
[9] L. Du, C. Shen, S. Jeon, and C. Gale, Probing initial baryon stopping and equation of state with rapidity-dependent directed flow of identified particles, Phys. Rev. C **108**, L041901 (2023).
[10] Y. Nara, H. Niemi, J. Steinheimer, and H. Stöcker, Equation of state dependence of directed flow in a microscopic transport model, Phys. Lett. B **769**, 543 (2017).
[11] Y. Nara, T. Maruyama, and H. Stoecker, Momentum-dependent potential and collective flows within the relativistic quantum molecular dynamics approach based on relativistic mean-field theory, Phys. Rev. C **102**, 024913 (2020).
[12] Y. Nara and H. Stoecker, Sensitivity of the excitation functions of collective flow to relativistic scalar and vector meson interactions in the relativistic quantum molecular dynamics model RQMD.RMF, Phys. Rev. C **100**, 054902 (2019).
[13] Y. Nara and A. Ohnishi, Mean-field update in the JAM microscopic transport model: Mean-field effects on collective flow in high-energy heavy-ion collisions at $\sqrt{s_{NN}}$ = 2–20 GeV energies, Phys. Rev. C **105**, 014911 (2022).
[14] Y. Nara, A. Jinno, K. Murase, and A. Ohnishi, Directed flow of Λ in high-energy heavy-ion collisions and Λ potential in dense nuclear matter, Phys. Rev. C **106**, 044902 (2022).
[15] Y. B. Ivanov and A. A. Soldatov, Correlation between global polarization, angular momentum, and flow in heavy-ion collisions, Phys. Rev. C **102**, 024916 (2020).
[16] N. S. Tsegelnik, E. E. Kolomeitsev, and V. Voronyuk, Helicity and vorticity in heavy-ion collisions at energies available at the JINR Nuclotron-based Ion Collider facility, Phys. Rev. C **107**, 034906 (2023).
[17] Z. F. Jiang, X. Y. Wu, S. Cao, and B. W. Zhang, Directed flow and global polarization in Au+Au collisions across energies covered by the beam energy scan at RHIC, Phys. Rev. C **107**, 034904 (2023).
[18] Z. F. Jiang, X. Y. Wu, S. Cao, and B. W. Zhang, Hyperon polarization and its relation with directed flow in high-energy nuclear collisions, Phys. Rev. C **108**, 064904 (2023).
[19] I. Karpenko and J. Cimerman, Directed flow and hyperon polarization at RHIC BES from multi-fluid dynamics, EPJ Web Conf. **296**, 04003 (2024).
[20] M. S. Abdallah *et al.* (STAR Collaboration), Flow and interferometry results from Au+Au collisions at $\sqrt{s_{NN}}$ = 4.5 GeV, Phys. Rev. C **103**, 034908 (2021).
[21] M. S. Abdallah *et al.* (STAR Collaboration), Disappearance of partonic collectivity in $\sqrt{s_{NN}}$ = 3 GeV Au+Au collisions at RHIC, Phys. Lett. B **827**, 137003 (2022).
[22] D. Oliinychenko, A. Sorensen, V. Koch, and L. McLerran, Sensitivity of Au+Au collisions to the symmetric nuclear matter equation of state at 2–5 nuclear saturation densities, Phys. Rev. C **108**, 034908 (2023).
[23] J. Steinheimer, A. Motornenko, A. Sorensen, Y. Nara, V. Koch, and M. Bleicher, The high-density equation of state in heavy-ion collisions: Constraints from proton flow, Eur. Phys. J. C **82**, 911 (2022).
[24] M. O. Kuttan, J. Steinheimer, K. Zhou, and H. Stoecker, QCD equation of state of dense nuclear matter from a bayesian analysis of heavy-ion collision data, Phys. Rev. Lett. **131**, 202303 (2023).
[25] A. Li, G. C. Yong, and Y. X. Zhang, Testing the phase transition parameters inside neutron stars with the production of protons and lambdas in relativistic heavy-ion collisions, Phys. Rev. D **107**, 043005 (2023).

[26] Z. M. Wu and G. C. Yong, Probing the incompressibility of dense hadronic matter near the QCD phase transition in relativistic heavy-ion collisions, Phys. Rev. C **107**, 034902 (2023).

[27] P. Parfenov, Model study of the energy dependence of anisotropic flow in heavy-ion collisions at $\sqrt{s_{NN}} = 2$–4.5 GeV, Particles **5**, 561 (2022).

[28] M. Mamaev and A. Taranenko, Toward the system size dependence of anisotropic flow in heavy-ion collisions at $\sqrt{s_{NN}} = 2 - 5$ GeV, Particles **6**, 622 (2023).

[29] N. Yao, A. Sorensen, V. Dexheimer, and J. Noronha-Hostler, Structure in the speed of sound: from neutron stars to heavy-ion collisions, arXiv:2311.18819.

[30] M. Kozhevnikova and Y. B. Ivanov, Light-nuclei production in Au+Au collisions at $\sqrt{s_{NN}} = 3$ GeV within a thermodynamical approach: Bulk properties and collective flow, Phys. Rev. C **109**, 014913 (2024).

[31] M. Kozhevnikova and Y. B. Ivanov, Light hypernuclei production in Au+Au collisions at $\sqrt{s_{NN}} = 3$ GeV within thermodynamic approach, Phys. Rev. C **109**, 034901 (2024).

[32] G. C. Yong, Phase diagram determination at fivefold nuclear compression, Phys. Lett. B **848**, 138327 (2024).

[33] S. N. Wei, W. Z. Jiang, and Z. Q. Feng, The influence of hyperon potential on neutron star matter and heavy-ion collisions, Phys. Lett. B **853**, 138658 (2024).

[34] C. T. Sturm *et al.* (KAOS Collaboration), Evidence for a soft nuclear equation of state from kaon production in heavy ion collisions, Phys. Rev. Lett. **86**, 39 (2001).

[35] W. Reisdorf *et al.* (FOPI Collaboration), Systematics of azimuthal asymmetries in heavy ion collisions in the 1 A GeV regime, Nucl. Phys. A **876**, 1 (2012).

[36] C. Fuchs, A. Faessler, E. Zabrodin, and Y. M. Zheng, Probing the nuclear equation of state by K+ production in heavy ion collisions, Phys. Rev. Lett. **86**, 1974 (2001).

[37] C. Hartnack, H. Oeschler, and J. Aichelin, Hadronic matter is soft, Phys. Rev. Lett. **96**, 012302 (2006).

[38] C. Hartnack, H. Oeschler, Y. Leifels, E. L. Bratkovskaya, and J. Aichelin, Strangeness production close to threshold in proton-nucleus and heavy-ion collisions, Phys. Rep. **510**, 119 (2012).

[39] H. Liu *et al.* (E895 Collaboration), Sideward flow in Au + Au collisions between 2*A* and 8*A* GeV, Phys. Rev. Lett. **84**, 5488 (2000).

[40] P. Chung *et al.* (E895 Collaboration), Antiflow of K_s^0 mesons in 6*A* GeV Au + Au collisions, Phys. Rev. Lett. **85**, 940 (2000).

[41] S. Pal, C. M. Ko, Z. Lin, and B. Zhang, Antiflow of kaons in relativistic heavy ion collisions, Phys. Rev. C **62**, 061903(R) (2000).

[42] P. Danielewicz, R. Lacey, and W. G. Lynch, Determination of the equation of state of dense matter, Science **298**, 1592 (2002).

[43] V. N. Russkikh and Y. B. Ivanov, Collective flow in heavy-ion collisions from AGS to SPS, Phys. Rev. C **74**, 034904 (2006).

[44] P. K. Sahu and W. Cassing, Differential flow of protons in Au+Au collisions at AGS energies, Nucl. Phys. A **712**, 357 (2002).

[45] M. Isse, A. Ohnishi, N. Otuka, P. K. Sahu, and Y. Nara, Mean-field effects on collective flows in high-energy heavy-ion collisions from AGS to SPS energies, Phys. Rev. C **72**, 064908 (2005).

[46] Y. B. Ivanov, V. N. Russkikh, and V. D. Toneev, Relativistic heavy-ion collisions within 3-fluid hydrodynamics: Hadronic scenario, Phys. Rev. C **73**, 044904 (2006).

[47] Y. B. Ivanov, Alternative scenarios of relativistic heavy-ion collisions: I. Baryon stopping, Phys. Rev. C **87**, 064904 (2013).

[48] A. Sorensen, K. Agarwal, K. W. Brown, Z. Chajecki, P. Danielewicz, C. Drischler, S. Gandolfi, J. W. Holt, M. Kaminski, C. M. Ko *et al.*, Dense nuclear matter equation of state from heavy-ion collisions, Prog. Part. Nucl. Phys. **134**, 104080 (2024).

[49] P. Batyuk, D. Blaschke, M. Bleicher, Y. B. Ivanov, I. Karpenko, S. Merts, M. Nahrgang, H. Petersen, and O. Rogachevsky, Event simulation based on three-fluid hydrodynamics for collisions at energies available at the Dubna nuclotron-based ion collider facility and at the facility for antiproton and ion research in Darmstadt, Phys. Rev. C **94**, 044917 (2016).

[50] P. Batyuk, D. Blaschke, M. Bleicher, Y. B. Ivanov, I. Karpenko, L. Malinina, S. Merts, M. Nahrgang, H. Petersen, and O. Rogachevsky, Three-fluid hydrodynamics-based event simulator extended by UrQMD final state interactions (THESEUS) for FAIR-NICA-SPSBES/RHIC energies, EPJ Web Conf. **182**, 02056 (2018).

[51] M. Kozhevnikova, Y. B. Ivanov, I. Karpenko, D. Blaschke, and O. Rogachevsky, Update of the three-fluid hydrodynamics-based event simulator: Light-nuclei production in heavy-ion collisions, Phys. Rev. C **103**, 044905 (2021).

[52] V. N. Russkikh and Y. B. Ivanov, Dynamical freeze-out in 3-fluid hydrodynamics, Phys. Rev. C **76**, 054907 (2007).

[53] Y. B. Ivanov and V. N. Russkikh, On freeze-out problem in relativistic hydrodynamics, Phys. At. Nucl. **72**, 1238 (2009).

[54] S. A. Bass, C. Hartnack, H. Stoecker, and W. Greiner, Out-of-plane pion emission in relativistic heavy ion collisions: Spectroscopy of Δ resonance matter, Phys. Rev. Lett. **71**, 1144 (1993).

[55] H. Heiselberg and A.-M. Levy, Elliptic flow and HBT in non-central nuclear collisions, Phys. Rev. C **59**, 2716 (1999).

[56] H. Liu, S. Panitkin, and N. Xu, Event anisotropy in high-energy nucleus-nucleus collisions, Phys. Rev. C **59**, 348 (1999).

[57] H. Sorge, Elliptical flow: A Signature for early pressure in ultrarelativistic nucleus-nucleus collisions, Phys. Rev. Lett. **78**, 2309 (1997).

[58] P. Danielewicz, R. A. Lacey, P.-B. Gossiaux, C. Pinkenburg, P. Chung, J. M. Alexander, and R. L. McGrath, Disappearance of elliptic flow: A new probe for the nuclear equation of state, Phys. Rev. Lett. **81**, 2438 (1998).

[59] Y. B. Ivanov and A. A. Soldatov, Elliptic flow in heavy-ion collisions at energies $\sqrt{s_{NN}} = 2.7$-39 GeV, Phys. Rev. C **91**, 024914 (2015).

[60] Y. B. Ivanov, Alternative scenarios of relativistic heavy-ion collisions: II. Particle production, Phys. Rev. C **87**, 064905 (2013).

[61] Y. B. Ivanov, Alternative scenarios of relativistic heavy-ion collisions: III. Transverse momentum spectra, Phys. Rev. C **89**, 024903 (2014).

[62] I. N. Mishustin, V. N. Russkikh, and L. M. Satarov, Fluid dynamical model of relativistic heavy ion collision, Sov. J. Nucl. Phys. **54**, 260 (1991).

[63] A. S. Khvorostukin, V. V. Skokov, V. D. Toneev, and K. Redlich, Lattice QCD constraints on the nuclear equation of state, Eur. Phys. J. C **48**, 531 (2006).

[64] Y. B. Ivanov and A. A. Soldatov, Equilibration and baryon densities attainable in relativistic heavy-ion collisions, Phys. Rev. C **101**, 024915 (2020).

[65] Y. Aoki, G. Endrodi, Z. Fodor, S. D. Katz, and K. K. Szabo, The order of the quantum chromodynamics transition predicted by

the standard model of particle physics, Nature (London) **443**, 675 (2006).
[66] S. Borsanyi, Z. Fodor, J. N. Guenther, R. Kara, S. D. Katz, P. Parotto, A. Pasztor, C. Ratti, and K. K. Szabo, QCD crossover at finite chemical potential from lattice simulations, Phys. Rev. Lett. **125**, 052001 (2020).
[67] Z. Fodor, Lattice QCD results at finite temperature and density, Nucl. Phys. A **715**, 319c (2003).
[68] F. Csikor, G. I. Egri, Z. Fodor, S. D. Katz, K. K. Szabo, and A. I. Toth, Equation of state at finite temperature and chemical potential, lattice QCD results, J. High Energy Phys. 05 (2004) 046.
[69] F. Karsch, E. Laermann, and A. Peikert, Quark mass and flavor dependence of the QCD phase transition, Nucl. Phys. B **605**, 579 (2001).
[70] W. Cassing and E. L. Bratkovskaya, Parton-hadron-string dynamics: An off-shell transport approach for relativistic energies, Nucl. Phys. A **831**, 215 (2009).
[71] Y. B. Ivanov and A. A. Soldatov, Entropy production and effective viscosity in heavy-ion collisions, Eur. Phys. J. A **52**, 367 (2016).
[72] Y. B. Ivanov, Baryon stopping as a probe of deconfinement onset in relativistic heavy-ion collisions, Phys. Lett. B **721**, 123 (2013).
[73] Y. B. Ivanov and D. Blaschke, Robustness of the baryon-stopping signal for the onset of deconfinement in relativistic heavy-ion collisions, Phys. Rev. C **92**, 024916 (2015).
[74] http://web-docs.gsi.de/~misko/overlap/interface.html
[75] H. G. Baumgardt, J. U. Schott, Y. Sakamoto, E. Schopper, H. Stoecker, J. Hofmann, W. Scheid, and W. Greiner, Shock waves and MACH cones in fast nucleus-nucleus collisions, Z. Phys. A **273**, 359 (1975).
[76] H. Stoecker, Collective flow signals the quark gluon plasma, Nucl. Phys. A **750**, 121 (2005).
[77] A. M. Poskanzer and S. A. Voloshin, Methods for analyzing anisotropic flow in relativistic nuclear collisions, Phys. Rev. C **58**, 1671 (1998).
[78] P. Danielewicz and G. Odyniec, Transverse momentum analysis of collective motion in relativistic nuclear collisions, Phys. Lett. B **157**, 146 (1985).
[79] M. Bleicher, E. Zabrodin, C. Spieles, S. A. Bass, C. Ernst, S. Soff, L. Bravina, M. Belkacem, H. Weber, H. Stoecker *et al.*, Relativistic hadron-hadron collisions in the ultrarelativistic quantum molecular dynamics model, J. Phys. G **25**, 1859 (1999).
[80] T. Song, L. Tolos, J. Wirth, J. Aichelin, and E. Bratkovskaya, In-medium effects in strangeness production in heavy-ion collisions at (sub)threshold energies, Phys. Rev. C **103**, 044901 (2021).
[81] W. Zwermann and B. Schurmann, The inclusive production of kaons in relativistic nucleus nucleus collisions based on transport theory, Nucl. Phys. A **423**, 525 (1984).
[82] V. N. Russkikh and Y. B. Ivanov, Kaon production in intermediate-energy nuclear collisions, Nucl. Phys. A **543**, 751 (1992).
[83] L. Tolos and L. Fabbietti, Strangeness in nuclei and neutron stars, Prog. Part. Nucl. Phys. **112**, 103770 (2020).
[84] W. Cassing, V. P. Konchakovski, A. Palmese, V. D. Toneev, and E. L. Bratkovskaya, Parton/hadron dynamics in heavy-ion collisions at FAIR energies, EPJ Web Conf. **95**, 01004 (2015).
[85] G. Q. Li, C. M. Ko, and X. S. Fang, Subthreshold anti-kaon production in nucleus-nucleus collisions, Phys. Lett. B **329**, 149 (1994).
[86] J. Schaffner, A. Gal, I. N. Mishustin, H. Stoecker, and W. Greiner, Kaon effective mass and energy in dense nuclear matter, Phys. Lett. B **334**, 268 (1994).
[87] E. E. Kolomeitsev, B. Kampfer, and D. N. Voskresensky, Kaon polarization in nuclear matter, Nucl. Phys. A **588**, 889 (1995).
[88] E. E. Kolomeitsev and D. N. Voskresensky, Negative kaons in dense baryonic matter, Phys. Rev. C **68**, 015803 (2003).
[89] http://ckp.nrcki.ru/
[90] http://hlit.jinr.ru/supercomputer_govorun/